

DOI: 10.1002/cctc.201402555

Insights into the Active Species of Nanoparticle-Functionalized Hierarchical Zeolites in Alkylation Reactions

Aida Grau-Atienza,^[a] Rafael Campos,^[b] Elena Serrano,^[a] Manuel Ojeda,^[b] Antonio A. Romero,^[b] Javier Garcia-Martinez,^{*,[a]} and Rafael Luque^{*,[b]}

Supported iron oxide nanoparticles have been incorporated onto hierarchical zeolites by microwave-assisted impregnation and mechanochemical grinding. Nanoparticle-functionalised porous zeolites were characterised by a number of analytical techniques such as XRD, N₂ physisorption, TEM, and surface acidity measurements. The catalytic activities of the syntheses-

used nanomaterials were investigated in an alkylation reaction. The results pointed to different species with varying acidity and accessibility in the materials, which provided essentially different catalytic activities in the alkylation of toluene with benzyl chloride under microwave irradiation, selected as the test reaction.

Introduction

Zeolites are microporous materials that have been investigated extensively over the past decades because of their important industrially related applications and implications in heterogeneously catalysed processes. Although they are used widely in many chemical processes, zeolites have been always limited by the narrow pore structure defined by their microporous crystalline framework.^[1–3] Many techniques have been used to introduce intracrystalline mesoporosity into zeolites to overcome the severe diffusion limitations in such materials for the conversion of bulky molecules.^[4–16] Among these treatments, desilication is one of the simplest and cheapest ways to introduce mesoporosity in zeolites.^[4–9] The treatment of zeolites (e.g. ZSM-5) with moderate Si/Al ratios (typically 25–50)^[5] with alkaline solutions allows the development of intracrystalline mesoporosity, which improves catalytic performance in hierarchical zeolites, especially in diffusion-limited processes.^[2,3]

An important step in the development of mesoporosity by desilication is a subsequent acid wash to remove the alumina debris formed during the first step in which silica is mostly extracted.^[17] Without this acid wash, the zeolite porosity is mainly blocked by the presence of amorphous alumina-rich debris species.^[18] Hierarchical zeolite-type materials have been report-

ed as highly active catalysts in a range of processes such as alkylations, acylations, related acid-catalysed processes and more recently biomass-derived transformations.^[19] However, there are only few studies that relate to the functionalisation of hierarchical zeolitic materials and insightful investigations on the nature of the active sites in heterogeneously catalysed processes.^[19,20]

Nanoparticles are active and stable catalysts once loaded onto an adequate support because of their small size, which confers them with a high surface area and a large amount of exposed active sites, and thereby good contact with reactants. Nanostructured heterogeneous catalysts are known to overcome the issues related to both homogeneous and heterogeneous catalytic systems, for example, they can be separated easily from reaction mixtures and show enhanced stability in comparison with traditional heterogeneous catalysts.^[21]

In this work, we have studied the effect of desilication (by alkali treatment) and subsequent acid treatment in the functionalisation of hierarchical ZSM-5 zeolites with different Si/Al ratios (15 and 40) with iron oxide nanoparticles. The surface acid properties of the materials have been investigated and correlated to the catalytic activity of the materials in the microwave-assisted alkylation of toluene with benzyl chloride. This process has been reported previously to be preferentially promoted by Lewis-acid sites,^[22] which is particularly useful if hierarchical zeolites are employed^[19b] as well as supported iron oxide nanomaterials.^[23a]

Results and Discussion

Hierarchical zeolite catalysts functionalised with iron oxide have been prepared by desilication and acid treatment of two commercial zeolites with the further incorporation of iron oxide nanoparticles under microwave-assisted irradiation and ball milling.

[a] A. Grau-Atienza, Dr. E. Serrano, Dr. J. Garcia-Martinez
Molecular Nanotechnology Lab.
Departamento de Química Inorgánica
Universidad de Alicante
Crtra. San Vicente s/n, E03690, Alicante (Spain)
Homepage: www.nanomol.es
E-mail: j.garcia@ua.es

[b] R. Campos, M. Ojeda, Dr. A. A. Romero, Dr. R. Luque
Departamento de Química Orgánica
Universidad de Córdoba
Edificio Marie Curie (C-3)
Ctra Nnal IV-A, Km 396, 14014, Córdoba (Spain)
Homepage: uco.es/~q62alsor
E-mail: q62alsor@uco.es

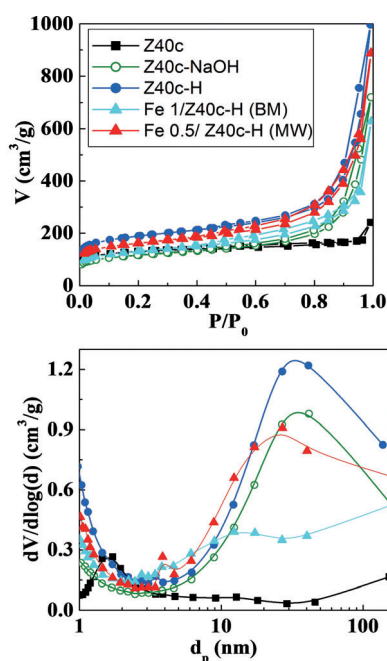


Figure 1. a) Representative N_2 adsorption/desorption isotherms at 77 K and b) the corresponding pore size distributions of samples with Si/Al = 40 (Z40c). Z40c-NaOH was treated with 0.4 M NaOH.

The mesoporous nature of the samples was investigated by N_2 adsorption/desorption at 77 K and TEM. Selected N_2 adsorption/desorption isotherms and the corresponding pore size distribution of the Z40c- and Z15c-based systems are shown in Figures 1 and 2, respectively. Based on the isotherms, the textural parameters were calculated and are listed in Table 1.

Parent zeolites (Z40c and Z15c) exhibit a type I isotherm with a narrow knee at low relative pressures in close agreement with its microporous structure. The desiccation treatment with NaOH induces a significant deterioration of the microporous structure, which is shown by the amount of N_2 adsorbed that decreases drastically at low relative pressures for samples with a higher NaOH concentration, that is, 0.8 M (Figures 1 and 2 and Table 1). As reported previously, the surface area and its relationship with the micropore and mesopore volumes is a good indication of the quality of the hierarchical systems.^[15,16,18] For example, the micropore volume of the parent Z15c zeolite was reduced from 0.14 to 0.11 and 0.01 $\text{cm}^3 \text{g}^{-1}$ after its alkaline treatment with 0.4 and

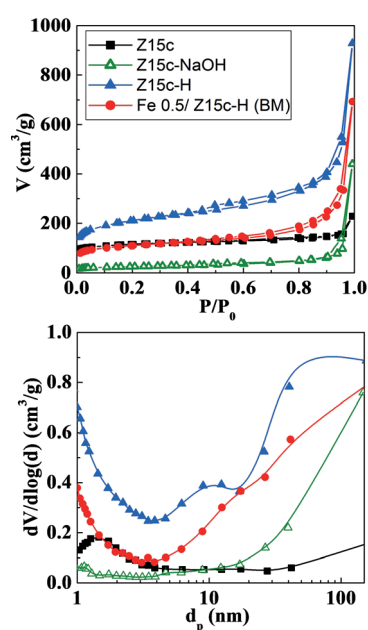


Figure 2. a) Representative N_2 adsorption/desorption isotherms at 77 K and b) the corresponding pore size distributions of samples with Si/Al = 15 (Z15c). Z15c-NaOH was treated with 0.8 M NaOH.

0.8 M NaOH, respectively. Accordingly, the BET area decreases upon reduction of the micropore volume (from 360 for Z15c to 290 and 85 $\text{m}^2 \text{g}^{-1}$ after treatment with 0.4 and 0.8 M NaOH, respectively), in addition to the increase of the mesopore volume with the alkaline treatment. The same trend has been observed for the Z40c zeolite, which indicates that the micropore reduction is related to the presence of amorphous Al-rich

Table 1. Chemical composition and textural parameters of the synthesised hierarchical catalysts compared to the parent zeolites before and after functionalisation with iron oxide nanoparticles.

Sample	Si/Al ^[a]	Fe ^[a] [wt %]	$S_{\text{BET}}^{\text{[d]}}$ [$\text{m}^2 \text{g}^{-1}$]	$S_{\text{meso}}^{\text{[e]}}$ [$\text{m}^2 \text{g}^{-1}$]	$V_{\text{micro}}^{\text{[e]}}$ [$\text{cm}^3 \text{g}^{-1}$]	$V_{\text{meso}}^{\text{[f]}}$ [$\text{cm}^3 \text{g}^{-1}$]	$V_{\text{poro}}^{\text{[g]}}$ [$\text{cm}^3 \text{g}^{-1}$]
Z40c	48.2 (40 ^[b])	–	410	210	0.14	0.16	0.30
Z40c-0.4NaOH	–	–	380	330	0.09	0.83	0.92
Z40c-H	50.0	–	610	440	0.16	1.13	1.29
Z40c-0.8NaOH	–	–	110	110	0.01	0.70	0.71
Z40c-0.8NaOH-HCl	–	–	430	425	0.06	0.74	0.80
Z15c	19.5 (15 ^[b])	–	360	190	0.14	0.13	0.27
Z15c-0.4NaOH	–	–	290	150	0.11	0.28	0.39
Z15c-0.4NaOH-HCl	–	–	500	370	0.15	0.44	0.59
Z15c-0.8NaOH	–	–	85	80	0.01	0.38	0.39
Z15c-H	20.0	–	690	590	0.16	0.89	1.05
Fe 0.5/Z40c-H (MW)	38.1	0.3/0.6 ^[c]	520	445	0.09	0.91	1.00
Fe 1/Z40c-H (BM)	42.3	0.7/1.8 ^[c]	425	365	0.07	0.64	0.71
Fe 1/Z40c-H (BM) 7 th use	44.6	0.8	–	–	–	–	–
Fe 0.5/Z15c-H (BM)	22.4	0.3/0.7 ^[c]	355	330	0.06	0.68	0.74

[a] Surface Si/Al mole ratio and Fe contents as determined by XPS after the samples were etched. [b] Theoretical value according to the manufacturer's specifications for the uncalcined samples. [c] Fe contents calculated by ICP-AES analysis of the filtrate after treatment of the samples with phosphoric acid and hydrochloric acid. [d] BET surface area was estimated by multipoint BET method using the adsorption data in the P/P_0 range of 0.05–0.30. [e] "External" surface area and micropore volume were obtained from the isotherms using the t-plot method. [f] Mesopore volume was obtained from the isotherms using the DFT method. [g] Pore volume was obtained from the isotherms at $P/P_0 = 0.95$.

fragments and points out the need of the acid washing in the materials.^[15,16,18] Desilicated samples, mainly Z40c-related systems, also showed enhanced N₂ adsorption at relatively high partial pressures ($P/P_0 > 0.8$), which is related to the development of interparticle meso-/macroporosity (also deduced from the pore size distributions shown in Figure 1).

After acid washing, all desilicated samples show N₂ adsorption at intermediate to high relative pressures related to the development of mesoporosity (Figures 1b and 2b), which is further confirmed by the increase in the mesopore volume of the desilicated samples compared with the parent zeolites (Figures 1 and 2 and Table 1). All samples show type IV isotherms with mesopore volumes between 0.44 and 1.13 cm³ g⁻¹ and micropore volumes similar to those of the parent zeolites, typical of hierarchical zeolites (Figures 1 and 2 and Table 1). Furthermore, an increase in both the BET surface area and the "external" surface area can be observed clearly in all the hierarchical zeolites, Z15c- and Z40c-based systems, which is usually ascribed to the increased mesopore volume. For example, for the Z15-derived samples, the starting Z15c has a BET surface area of 360 m² g⁻¹, of which 190 m² g⁻¹ is the contribution of the "external" surface area from t-plot analysis, that is, surfaces areas from the true crystal external surfaces and from internal voids larger than micropores.^[15,16] The hierarchical Z15c-H zeolite exhibited a BET surface area of 690 m² g⁻¹, which is approximately 330 m² g⁻¹ higher than that of the parent sample. A contribution of approximately 590 m² g⁻¹ is derived from the "external" surface of the hierarchical zeolite, which is approximately four times higher than that of parent Z15c, in agreement with the increase of mesopore volume (0.13 vs. 0.89 cm³ g⁻¹).

TEM images also showed structural features of hierarchical porous zeolites after NaOH treatment (desilication and opening of the highly crystalline zeolite particles) followed by HCl treatment (Figure 3).

Two different sets of functionalised materials were synthesised by microwave-assisted (MW) and dry milling (BM) incorporation of iron oxide nanoparticles. The synthesised materials (Table 1 and Figures 1 and 2) possessed similar textural properties, in terms of surface area and pore volume, to the parent hierarchical zeolites.

Upon the incorporation of iron oxide nanoparticles, a partial blockage of the micropores (0.16 vs. 0.06–0.09 cm³ g⁻¹) was observed in the hierarchical zeolites, which can be mainly attributed to iron migration into the micropores (to cause blockage) as well as the partial collapse of the porous structure,^[23b,25] as observed in the pore size distributions shown in Figures 1 and 2. In any case, a preferential deposition of iron oxide nanoparticles takes place on the external surface of the materials (for both MW and BM methodologies) as later confirmed in the catalytic activity results. The adsorption at $P/P_0 > 0.6$, which is characteristic of textural interparticle meso-/macroporosity, remains almost identical to those of Z15c-H and Z40c-H for 0.5 wt% Fe catalysts (Figures 1 and 2 and Table 1).

Both methodologies were effective in the incorporation of Fe quantities close to the theoretical loadings (0.5–0.7 wt% actual loading for 0.5 wt% Fe materials and 1.8 wt% for 1 wt%

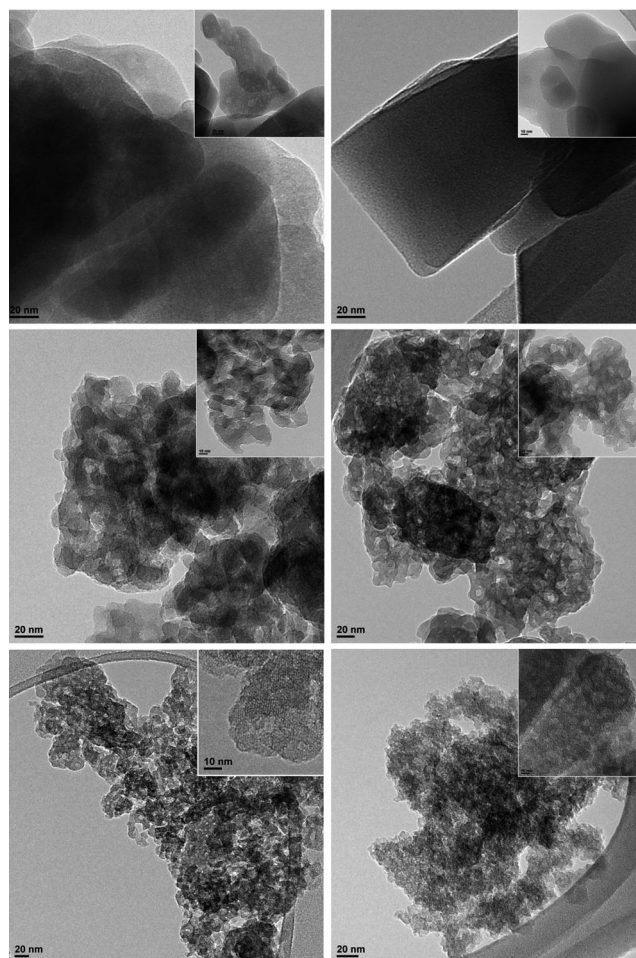


Figure 3. TEM micrographs of: (top left) Z40c, (top right) Z15c, (middle left) Z40c-0.4NaOH, (middle right) Z15c-0.8NaOH, (bottom left) Z40c-H and (bottom right) Z15c-H. Scale bar = 20 nm. Scale bar in the inset = 10 nm, except for Z40c, the scale bar of which corresponds to 20 nm.

Fe materials as measured by inductively coupled plasma atomic emission spectroscopy (ICP-AES); Table 1). The surface Fe content (measured by X-ray photoelectron spectroscopy (XPS) with and without etching) was determined to be approximately a third of the total Fe content in the materials (Table 1). Surface Si/Al molar ratios (also measured by XPS) remained almost unchanged upon Fe incorporation. The Fe distribution was also rather homogeneous on the hierarchical zeolites (even in materials reused several times in the alkylation reaction) as demonstrated clearly in the SEM mapping and TEM images (Figures 4 and 5, respectively), although the presence of iron oxide nanoparticles could not be distinguished clearly by TEM (Figure 5).

Representative XPS spectra of the Fe-containing materials in the region that corresponds to the Fe2p peak are shown in Figure 6. As shown in the XPS spectra of Fe 1/Z40c-H (BM), the binding energies (BEs) of the Fe2p_{3/2} and Fe2p_{1/2} peaks are located at approximately 711 and 725 eV, respectively, typical of oxidised Fe³⁺ species (Figure 6, top left).^[23,26] The peak at BE = 711 eV is traditionally assigned in the literature to Fe³⁺ species, whereas the shoulder at approximately BE = 719 eV belongs to

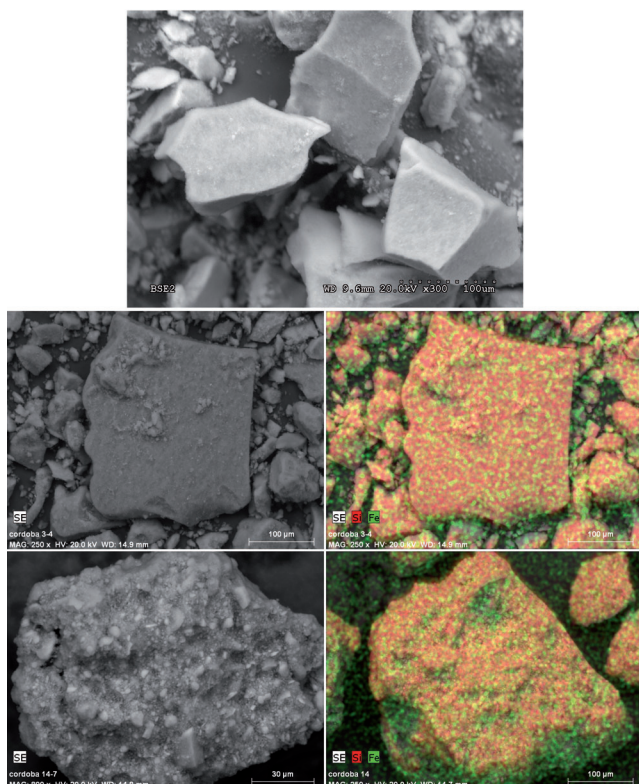


Figure 4. SEM micrographs of: (top) Z40c-H, (middle) Fe 0.5/Z40c-H (MW) and (bottom) reused Fe 1/Z40c-H BM (after seven catalytic cycles).

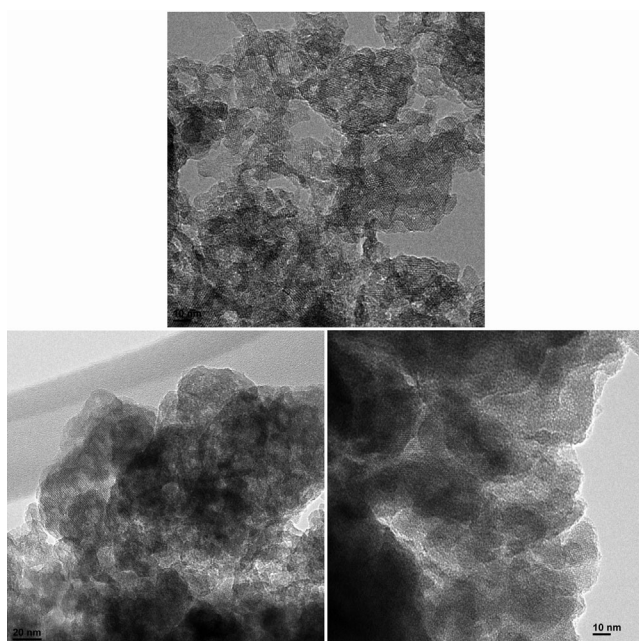


Figure 5. TEM micrographs of: (top) Fe 0.5/Z40c-H (MW), scale bar = 10 nm, (bottom left) Fe 1/Z40c-H (BM), scale bar = 20 nm, and (bottom right) reused Fe 1/Z40c-H (BM) (seven catalytic cycles), scale bar = 10 nm.

a satellite peak, characteristic of Fe^{3+} species seen in Fe_2O_3 materials.^[23,26]

Therefore, the XPS results confirmed the presence of fully oxidised Fe species (mostly Fe^{3+} species, hematite phase) with

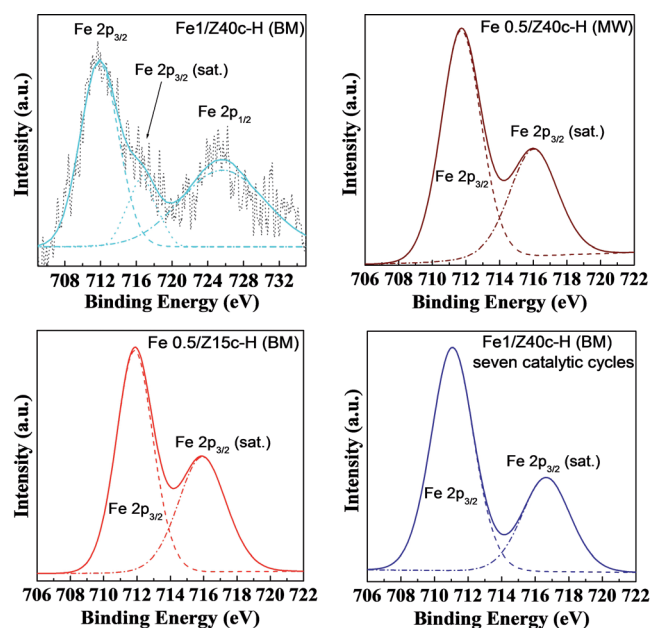


Figure 6. Representative XPS spectra of Fe-containing Z40c and Z15c materials in the region of the $\text{Fe } 2p_{3/2}$ peak. For Fe 1/Z40c-H (BM), the whole Fe 2p XPS spectrum is shown, which includes the measured data (black points). BEs [eV] were corrected with respect to the C 1s peak (284.6 eV).

similar profiles irrespective of the Fe loading (0.5 or 1 wt% Fe), the methodology employed for the preparation of the materials and even after several reuses in the selected alkylation process, in good agreement with supported iron oxide nanoparticle materials reported previously.^[23,26]

The results of the surface acidity characterisation of the materials are included in Table 2 and Figure 7. The parent calcined zeolites possess typical acidities reported previously for ZSM-5 materials, with a significant contribution of Lewis and Brønsted (major) acid sites.^[25,27–30] Interestingly, the different treatments of the parent ZSM-5 gave rise to materials with essentially different surface acid properties although no clear correlation between acidity and textural properties could be made (see Table 1 and Table 2). The development of mesoporosity in ZSM-5 improved the accessibility of 2,6-dimethylpyridine (DMPY) to Brønsted acid sites compared to the parent zeolites, in good agreement with previous results.^[25,28–30] However, in contrast to previous studies, desilication of the parent zeolites by NaOH treatment (Z40c-XNaOH and Z15c-YNaOH samples) resulted in significant pore blockage as demonstrated by the N_2 physisorption studies, which hindered the accessibility of probe molecules (even pyridine; PY) to acid sites significantly (Table 1 and Table 2). The incorporation of iron oxide nanoparticles in alkali-treated materials by the BM methodology gave materials with virtually no acidity (with the exception of Fe 0.5/Z40c-0.4NaOH-BM), in agreement with the negligible accessible surface (Table 2). The MW deposition of Fe onto alkali-treated materials was only attempted for Z15c-0.8NaOH and led to an essentially similar low-acidity material that was not further investigated (not shown).

The accessibility of probe molecules increased remarkably after the acid-washing treatment due to their excellent textural

Table 2. Surface acidity (measured using PY and DMPY as probe molecules at 200 °C) of the different catalysts synthesised in this work.

Catalyst	PY [$\mu\text{mol g}^{-1}$] (B+L)	DMPY [$\mu\text{mol g}^{-1}$] (B)	Lewis acidity [$\mu\text{mol g}^{-1}$] (L)
Z40c	218	14	204
Fe 0.5/Z40c (MW)	200	51	149
Fe 0.5/Z40c (BM)	309	174	135
Z15c	529	285	244
Fe 0.5/Z15c (MW)	470	199	271
Fe 0.5/Z15c (BM)	347	128	219
Z40c-0.4NaOH	30	6	24
Z40c-0.8NaOH	< 10	–	< 10
Fe 0.5/Z40c-0.4NaOH (BM)	145	32	113
Z15c-0.4NaOH	< 10	–	< 10
Z15c-0.8NaOH	25	7	18
Fe 0.5/Z15c-0.8NaOH (BM)	30	2	28
Z40c-H	264	249	15
Fe 0.5/Z40c-H (MW)	291	238	53
Fe 0.5/Z40c-H (BM)	240	151	89
Fe 1/Z40c-H (BM)	322	250	72
Z15c-H	367	355	12
Fe 0.5/Z15c-H(MW)	362	320	42
Fe 0.5/Z15c-H (BM)	329	294	35

Lewis acidity was calculated as the difference between the PY and DMPY values by assuming that all DMPY titrates Brønsted sites (B) selectively and PY titrates both Brønsted and Lewis acid sites in the materials (B+L, see Experimental Section).

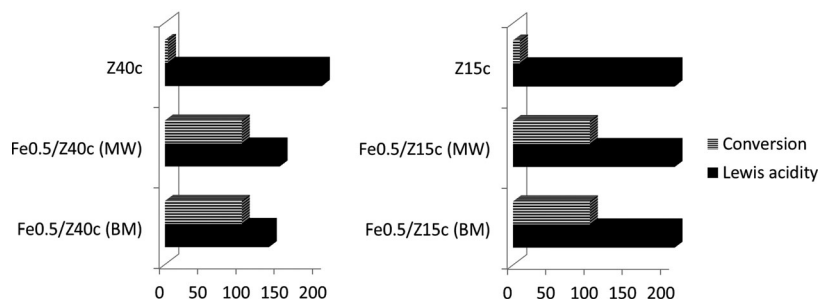


Figure 7. Comparison of acidity [$\mu\text{mol g}^{-1}$] versus catalytic conversion [%] for (Fe)Z40c and (Fe)Z15c. Reaction conditions: 2 mL toluene, 0.2 mL benzyl chloride, 0.025 g catalyst, microwave irradiation, 300 W, 5 min.

properties (Table 2). Interestingly, subsequent HCl washing of both Z40c-NaOH and Z15c-NaOH materials generated almost exclusively Brønsted acid sites, which were only slightly increased (together with Lewis acidity) in Fe-containing materials (Table 2, Z-NaOH-HCl and Fe 0.5/Z-NaOH-HCl). In this particular case, the Fe incorporation methodology (MW or BM) did not have a significant effect on the acidity of the systems.

Upon full characterisation, the catalytic activity of all synthesised materials was investigated in the alkylation of toluene with benzyl chloride as a model reaction promoted by Lewis acidity.^[22] The selected model reaction provided interesting insights into the location of the active sites (Lewis and Brønsted) as well as the effect of the generated porosity/treatment for ZSM-5 materials. The results included in Table 3 show that blank runs (in the absence of catalyst) provided negligible conversion to products in the systems as expected. Similarly, no

conversion in the proposed alkylation reaction was obtained for calcined microporous ZSM-5 materials regardless of their Si/Al ratios and despite their high total and Lewis acidities (Tables 2 and 3). The negligible conversion to product for the microporous materials is related to their small pores that may be able to accommodate the starting materials (toluene and benzyl chloride) but not the alkylated *ortho*-, *meta*- and even *para*-diphenylmethane, which most probably remain inside the zeolite pores. These results are in good agreement with literature reports for similar systems.^[19,27,31]

Gratifyingly, the incorporation of iron oxide nanoparticles into microporous Z40c and Z15c [Fe0.5 and Fe1/Z40c (MW) and (BM)] provided quantitative conversion to alkylated products under identical reaction conditions regardless of the methodology utilised for Fe deposition (MW or BM; Table 3). Such excellent activities were observed for Fe-containing materials, which generally exhibited reduced Lewis (and total) acidities compared with parent Z40c and Z15c (Figure 7).

These important differences can be correlated to the development of highly active and accessible Lewis acid sites on the external surface of the zeolites, which are able to catalyse the alkylation reaction efficiently. Similar catalysts were prepared on mesoporous Si-MCM-41 and MSU-X silicas, that is, with a 0.5 wt % Fe loading and using both MW and BM techniques. In both cases, the catalysts were not active for this reaction,

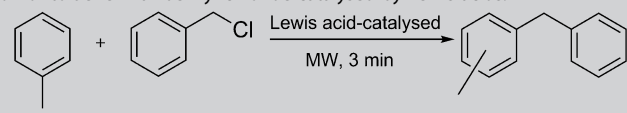
which thus supports the role of acidity on the catalytic activity of these samples. The presence of nanoparticles deposited preferentially on the external surface (BM)^[23b,32] as well as a contribution within the pores of porous materials (MW) has been demonstrated previously.^[23] The incorporation of Fe also influences the Al environment critically through an observed synergetic effect between Al and Fe.^[23a]

Alkali treatment of Z40c and Z15c rendered pore-blocked materials with significantly reduced

textural properties and total acidity (Brønsted+Lewis), which are catalytically inactive in the alkylation reaction (Table 3). Unexpectedly, the incorporation of Fe into Z40c and Z15c-NaOH materials rendered materials with an inferior total (and Lewis) acidity, which were completely inactive in the investigated Lewis-acid-catalysed alkylation regardless of the deposition approach (MW or BM; Table 3). These results were rather unexpected so further studies were performed to gain a better understanding of the synthesised materials.

The significantly different XRD patterns of BM-incorporated Fe 0.5/Z15c-NaOH and Fe 0.5/Z15c-H materials are compared in Figure 8. Several crystalline diffraction lines were observed at $2\theta = 23.3, 23.5, 24.5, 30.5$ and 45.4° in the pattern of Fe 0.5/Z15c-H (blue line, Figure 8). These correspond to an aluminium silicate ZSM-5 structure.^[7,20] No lines that correspond to iron oxide nanoparticles could be visualised in this material be-

Table 3. Catalytic activity of hierarchical zeolite materials in the microwave-assisted alkylation of toluene with benzyl chloride catalysed by Lewis acids.



Catalyst	Conv. [%] Total	Select. [%]		
		<i>meta</i>	<i>ortho</i>	<i>para</i>
Blank (no catalyst)	–	–	–	–
Z40c	< 5	11	40	48
Fe 0.5/Z40c (BM)	> 99	8	43	49
Fe 0.5/Z40c (MW)	> 99	8	43	49
Z15c	< 5	15	47	38
Fe 0.5/Z15c (BM)	> 99	15	36	49
Fe 0.5/Z15c (MW)	> 99	18	35	47
Z40c-NaOH	–	–	–	–
Fe 0.5/Z40c-NaOH (BM)	< 10	8	42	51
Z15c-NaOH	< 5	–	41	59
Fe 0.5/Z15c-NaOH (BM)	–	–	–	–
Z40c-H	–	–	–	–
Fe 0.5/Z40c-H (BM)	> 99	10	39	51
Fe1/Z40c-H (BM)	87	7	43	50
reused Fe1/Z40c-H (BM) (seven catalytic uses)	> 99	10	45	45
Fe/Z40c-H (MW)	97	8	44	48
Z15c-H	–	–	–	–
Fe 0.5/Z15c-H (BM)	> 99	10	44	46
Fe 0.5/Z15c-H (MW)	97	12	40	48

Reaction conditions: 2 mL toluene, 0.2 mL benzyl chloride, 0.025 g catalyst, microwave irradiation, 300 W, 5 min.

cause of the low Fe loading, but the presence of such Fe₂O₃ species was confirmed by XPS (Figure 6). However, most of these reflections were not present in the XRD pattern of Fe 0.5/Z15c-NaOH (green line, Figure 8), which exhibited a broad amorphous band centred at 2θ = 25° and various intense diffraction lines that correspond to the formation of an iron aluminate phase (2θ = 31.8, 37.5—maximum intensity that corresponds to the (311) diffraction line—and 44.6°),^[33,34] with no evidence of the distinctive lines of iron oxide nanoparticles. The formation of the iron aluminate phase has been reported previously to be generated from Fe-Al₂O₃ composites under similar ball-milling metallurgy processes from reactive sintering between Fe and Al₂O₃.^[33,34]

Iron aluminate does not have any acidity, which can explain the observed reduced acidity upon Fe incorporation in these materials, and consequently, such a material is not expected to have any catalytic activity in the alkylation reaction.^[33,34] To further support this theory, iron aluminate prepared following a literature method^[34] was also tested in the alkylation and showed no conversion to products under the investigated conditions. The formation of this inert inorganic iron aluminate phase was induced by the reac-

tion of alumina debris formed upon alkali treatment with the Fe precursor under BM conditions (reactive milling).

The HCl treatment of Z40c and Z15c-NaOH materials generally improved both the total and particularly the Brønsted acidity in the final hierarchically porous Z40c-H and Z15c-H materials, which exhibited significantly improved and more accessible acid sites (Table 2). However, these materials possessed essentially Brønsted acid sites hence exhibited no conversion in the toluene alkylation with benzyl chloride (Table 3 and Figure 9). Lewis acid sites provided by the extra-framework Al phases in calcined zeolites were generally found to be inactive in the tested reaction.

Upon Fe incorporation, Lewis acidity is created in the materials from the deposition of iron oxide nanoparticles that lead to highly active and accessible active sites on the surface of the hierarchical zeolites, which are able to catalyse the alkylation reaction efficiently to give high yields (>90%; Table 3 and Figure 9). Interestingly, the Fe 0.5/Z40c-H and Fe 0.5/Z15c-H materials exhibited very similar acid properties to those of the parent Z40c-H and Z15c-H materials, with the exception of the generated Lewis acidity upon the incorporation of iron oxide nanoparticle (Figure 9). Product selectivity was similar for all Fe-containing catalytically active materials with a slightly

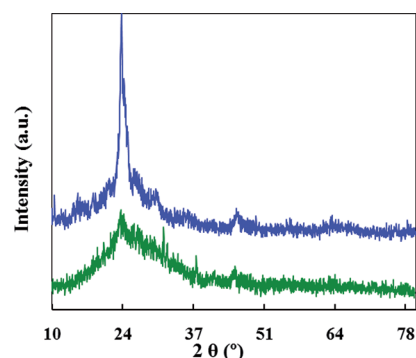


Figure 8. Comparison of the XRD patterns of Fe 0.5/Z15c-H (blue line) and Fe 0.5/Z15c-NaOH (green line). The XRD patterns show the presence of an FeAl₂O₄ phase, with its distinctive (311) diffraction line at 2θ = 37.5°.^[33,34]

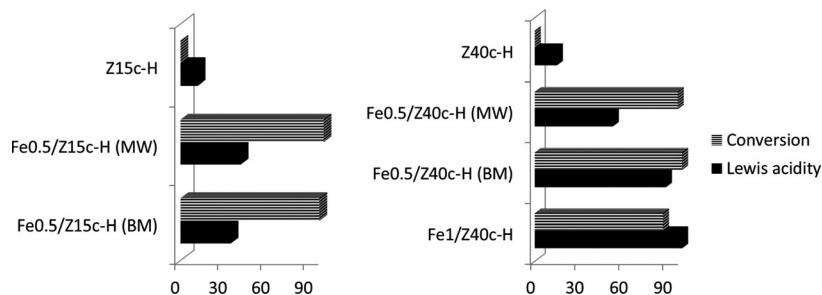


Figure 9. Comparison of acidity [μmol g⁻¹] versus catalytic conversion [%] for (Fe)Z40c-H and (Fe)Z15c-H. Reaction conditions: 2 mL toluene, 0.2 mL benzyl chloride, 0.025 g catalyst, microwave irradiation, 300 W, 5 min.

preferential selectivity to the *para* derivative as expected (less sterically hindered product; Table 3). The observed differences between inactive iron oxide nanoparticles on desilicated NaOH-treated zeolites and their hierarchical counterparts is believed to be related to Fe-Al synergy reported previously^[23,35,36] in this case with the acidity of the zeolite support. In the case of Fe-containing desilicated zeolites, both porosity and acidity are blocked (Figure 10). Fe incorporation leads to iron oxide nanoparticle species of relatively low acidity [Table 2; Fe 0.5/Z40c-0.4NaOH (BM)] that are poorly active and unable to promote the reaction to a large extent. Upon acid washing, both the porosity and acidity influence an improved interaction between Fe-Al to bring back the synergistic role of acidity and thus lead to highly active materials. This is also the case for Fe-containing microporous zeolites (Table 3 and Figure 10) in which Fe-Al synergism provides high activities in the alkylation of toluene with benzyl chloride.

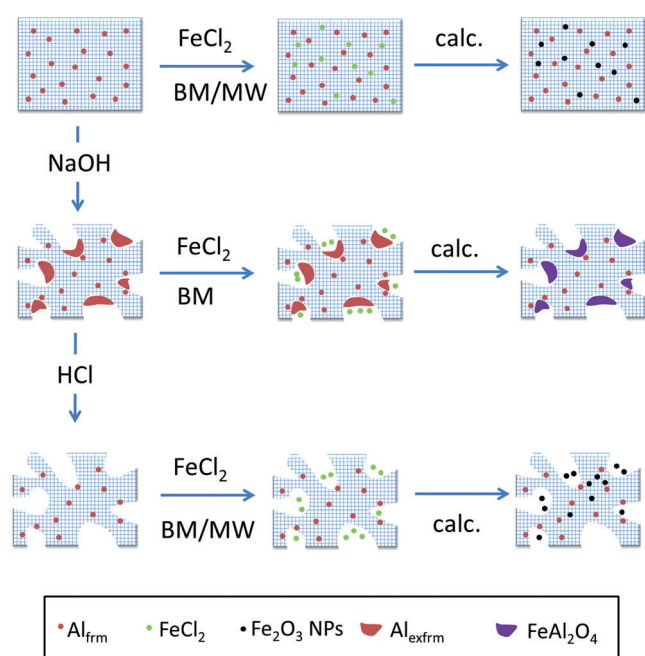


Figure 10. Schematic representation of the synthesis and proposed structures of Fe/Z40c and Fe/Z15c (top), Fe/Z40c-NaOH and Fe/Z15c-NaOH (middle) and Fe/Z40c-H and Fe/Z15c-H (bottom).

A strict catalytic activity comparison between parent versus hierarchical zeolites was conducted to prove any advantages of the developed mesoporosity for the selected process. With this purpose, 1 and 3 min microwave experiments were performed for both Fe 0.5/Z15c-H (BM) and Fe 0.5/Z15c (BM) as well as for MW-prepared materials. The results (not shown) indicated only a slightly superior conversion for hierarchical Fe-containing Z15c-H materials compared to the parent microporous counterparts [that is, 52% conversion for Fe 0.5/Z15c-H (BM) vs. 43% conversion for Fe 0.5/Z15c (BM), microwave 300 W, 3 min reaction under identical conditions to those stated in Table 3]. The apparent slight difference in activity (which could be attributed to the observed migration of iron

oxide species into the zeolite micropores upon Fe incorporation; Table 1) might actually be significant if we take into account the differences in Lewis acidity between the two materials ($219 \mu\text{mol g}^{-1}$ for microporous vs. $35 \mu\text{mol g}^{-1}$ for Fe-containing mesoporous Z15c-H; Table 2). The explanation for this effect is not trivial and will require further investigations, particularly as the proposed assumption for Lewis acidity may not be correct for the hierarchical zeolites. In any case, current findings (if we leave aside the consideration of Lewis acidity) seem to indicate that the developed mesoporosity in the materials does not add significant advantages in terms of catalytic activity for the particular alkylation reaction selected.

The findings obtained for the different systems and plausible explanations for the different Fe-containing materials are summarised and depicted in Figure 10. The synthesised materials comprise a) active iron oxide nanoparticles that are incorporated predominantly on the external surface of the untreated ZSM-5 zeolites by BM or MW (Fe/Z40c and Fe/Z15c), b) an iron aluminate phase from the reactive milling of Fe and extra-framework alumina species upon desilication in alkali-treated Z40c and Z15c-NaOH materials and c) a combination of highly active iron oxide nanoparticles on the external surface (plus some contribution within the pores) of acid-reconstituted ZSM-5 hierarchical Fe/Z40c-H and Fe/Z15c materials.

The reusability of the Fe-containing materials was tested in the proposed alkylation reaction. The SEM and TEM analysis, textural properties and Fe content (Table 2 and Figures 3 and 5) support the stability of the Fe-incorporated hierarchical materials, the activities of which were almost unchanged after seven catalytic cycles (see Table 3). Regeneration by calcination at 400°C for 2 h was conducted after the first run (a significant loss of activity was observed, up to 70% of the initial conversion) to preserve such activity. Upon calcination after the first reuse, Fe1/Z40c-H (BM) provided remarkable catalytic activity, even slightly superior to that in the first catalytic run, after subsequent runs with up to six reuses (Table 3). The conditioning of the catalyst after every reuse (after the first calcination) comprised a simple washing step with ethanol and acetone and drying overnight at 110°C before reuse in the alkylation reaction.

A hot filtration test was conducted half-way through the reaction (typically after 3 min reaction at $\approx 45\text{--}55\%$ conversion) to ascertain the presence of leached Fe species in the solution. Experiments were performed similarly to all catalytic reactions (Table 3), and the catalyst was removed by filtration quickly immediately after the microwave was stopped. The catalyst was put into a clean vial with fresh substrates (benzyl chloride and toluene) and subjected to another reaction to provide essentially identical yields of diphenylmethanes compared to the conventional reactions.

Importantly, after the catalyst was removed, the reaction filtrate was further reacted for 60 min under microwave irradiation. A negligible increase in conversion was observed in repeated runs (i.e., from 55% conversion in the original filtrate to 53–60% conversion after 60 min), which supports the truly heterogeneous nature of the catalytic system. Furthermore, inductively coupled plasma mass spectrometry (ICP-MS) of the

filtrate after 60 min under microwave irradiation showed no detectable quantities of Fe in the solution (< 0.5 ppm), in good agreement with the stability of similar Fe-containing materials demonstrated previously.^[36,37] These results were again in good agreement with the XPS data for the Fe content of Fe1/Z40c-H (BM) after seven uses.

Conclusion

The alkylation of toluene with benzyl chloride was selected to demonstrate the inherent advantages of nanoparticle-supported systems prepared under a new mechanochemical deposition method as well as a microwave-assisted protocol, which allow the design of stable and active zeolites that contain iron oxide nanoparticles for a series of useful catalytic transformations.^[35,36] An interesting synergetic effect between Fe and Al in the zeolites was observed for the synthesised materials in the alkylation of toluene with benzyl chloride, in which the Lewis acid sites of extra-framework Al phases in calcined zeolites are generally inactive. The Fe-containing zeolites were also remarkably stable under the investigated conditions and were reusable up to seven times with extremely stable Fe species in their structure (no Fe leaching and no significant changes in Fe species were observed upon reuse).

The Fe-containing materials prepared in line with previous reports proved that the generation of iron oxide nanoparticles on mesoporous aluminosilicate supports can enhance the catalytic activity of the final catalysts significantly.^[23a,35–37]

Experimental Section

Materials and methods

Two commercial MFI zeolites, CBV8014 (Zeolyst International, Si/Al molar ratio = 40) and CBV3024E (Zeolyst International, Si/Al molar ratio = 15), were used as starting materials after calcination at 550 °C for 5 h in air (rate of 100 °C h⁻¹). These are denoted as Z40c and Z15c, in which Z stands for the type of zeolite (ZSM-5), the number (40 or 15) refers to the Si/Al ratio according to the manufacturer's specifications, and the letter c refers to the calcined material.

Post-synthetic treatments

Post-synthetic desilication treatment was conducted following the methodology reported by Groen et al.^[18,24] in which zeolites were treated with different concentrations of NaOH solution (0.4 and 0.8 M) and washed subsequently with HCl to obtain hierarchical ZSM-5 porous zeolites.

Typically, the parent zeolite (3.3 g; Z40c or Z15c) was stirred magnetically at 600 rpm and 65 °C in an aqueous solution of NaOH (100 mL, 0.4 or 0.8 M) for 30 min. The material was collected by filtration and washed thoroughly with distilled water. Alkali-treated materials are denoted as Z40c-XNaOH and Z15c-YNaOH, in which Z stands for the type of zeolite (ZSM-5), the number (40 or 15) refers to the Si/Al molar ratio according to the manufacturer's specifications, the letter c refers to the calcined material and X or Y refers to the concentration of alkali utilised to treat the samples (0.4 and 0.8 M NaOH).

Subsequently, the alkaline-treated samples were washed with HCl (0.1 M) to remove amorphous Al-rich debris. Each sample (1 g; Z40c-XNaOH or Z15c-YNaOH) was stirred in aqueous HCl (100 mL; 0.1 M) for 6 h at 65 °C. The solid was collected by filtration and washed with distilled water. Treatment yields varied from 14–20%. Hierarchical ZSM-5 materials after acid washing are denoted as Z40c-XNaOH-HCl and Z15c-YNaOH-HCl. For brevity, two samples, Z40c-0.4NaOH-HCl and Z15c-0.8NaOH-HCl, are denoted Z40c-H and Z15c-H, respectively, in the manuscript. Z40c-H denotes a hierarchical ZSM-5 porous zeolite calcined with an initial Si/Al molar ratio of 40 obtained after treatment with a 0.4 M NaOH solution and washed with a 0.1 M solution of aqueous HCl. Similarly, Z15c-H corresponds to a hierarchical ZSM-5 porous zeolite calcined with an initial Si/Al 15 ratio obtained after washing with a 0.8 M NaOH solution (optimum conditions) and reconstituted with a 0.1 M solution of aqueous HCl. The NaOH concentrations were selected to provide good textural and acid properties in the final materials.

Synthesis of nanoparticle-functionalised mesoporous zeolites

Microwave-assisted deposition of Fe-containing materials

Materials were prepared according to a methodology reported previously.^[23a] Typically, zeolite (0.5 g), ethanol/water (1:2, 2.0 mL) and the target quantity of FeCl₂·6H₂O to reach a theoretical 0.5 wt% Fe content in the material were microwaved by using a CEM-DISCOVER reactor for 15 min at 300 W (maximum power output), which led to a maximum temperature of 100–110 °C (power-control method). The solids were collected by filtration and washed thoroughly with ethanol and acetone, oven dried overnight at 100 °C and calcined in air at 400 °C for 2 h to stabilise iron oxide nanoparticles on the zeolites before their use in the alkylation reaction.^[35] Materials are denoted as Fe/Z (MW) derived materials in which Fe represents a theoretical Fe incorporation of 0.5 wt% in the final material, Z refers to the zeolitic material synthesised, and MW indicates the microwave-assisted incorporation of the metal.

Mechanochemical preparation of Fe-containing materials

Materials were also prepared using an innovative mechanochemical protocol developed recently in our group.^[23b] Typically, the pre-formed ZSM-5 material (2 g) was ground with the target quantity of metal precursor (FeCl₂·6H₂O, Sigma-Aldrich) in the solid phase to achieve a 0.5 wt% Fe loading in the final material (unless otherwise stated). The mechanochemical protocol was performed by using a planetary ball mill (Retsch PM 100 model) under conditions optimised previously (10 min milling at 350 rpm). The obtained materials were calcined in air at 400 °C for 2 h. Materials are denoted as Fe 0.5 or Fe 1/Z (BM), in which Fe 0.5 or Fe 1 stand for a theoretical Fe incorporation of 0.5 or 1 wt%, respectively, in the final material (unless otherwise stated), Z refers to the zeolitic material synthesised, and BM stands for ball-milling incorporation of the metal oxide nanoparticles.^[23b]

Characterisation

The porosity of the materials was measured by N₂ adsorption at 77 K by using an AUTOSORB-6 apparatus. Samples were degassed for 5 h at 373 K at 5.10⁻⁵ bar before measurement. The BET surface area was estimated by using the multipoint BET method and the adsorption data in the relative pressure (*P/P*₀) range of 0.05–0.30. The pore size distribution was calculated from the adsorption

branch of the N₂ isotherms using the Barret–Joyner–Halenda (BJH) method. The mesoporous volume was calculated from the cumulative pore volume distribution curve. The micropore volume was calculated by the t-plot method.

The morphology and structure of the materials was investigated by TEM and SEM. TEM micrographs were obtained by using a JEM-2010 microscope (JEOL, 200 kV, 0.14 nm resolution). Samples were prepared by dripping a sonicated suspension of the materials in ethanol on a carbon-coated copper grid. SEM analysis was performed on gold-coated samples by using a JSM-840 microscope (JEOL).

The electronic state of Fe species and the Si/Al molar ratio of the samples after the alkaline and acid treatments were determined by XPS by using a VG-Microtech Multilab instrument equipped with MgK_α ($h\nu = 1253.6$ eV) radiation and a pass energy of 50 eV. The BEs [eV] were corrected with respect to the C 1s peak (BE = 284.6 eV). Samples were submitted to an etching treatment by using an Ar⁺ ion source operating at 3 kV at a current of 30 mA for 30 s twice to clean the specimen surface.

The metal content was also determined by ICP-AES by using a PerkinElmer 7300 DV spectrometer. Samples were dissolved in phosphoric acid and hydrochloric acid, and undissolved matter was removed by filtration before analysis.

PY and DMPY titration experiments were conducted at 200 °C by the gas-phase adsorption of the basic probe molecules using a pulse chromatographic titration methodology.^[27] Briefly, probe molecules (typically 1–2 μL) were injected in very small amounts (to approach conditions of gas-chromatography linearity) into a gas chromatograph through a microreactor in which the solid acid catalyst was placed. The basic compounds are adsorbed until complete saturation, from which the probe molecules in the gas phase are detected in the GC. The quantity of probe molecule adsorbed by the solid acid catalyst can be quantified easily. To distinguish between Lewis and Brønsted acidity, the assumption was made that all DMPY titrates Brønsted sites selectively (methyl groups hinder the coordination of N atoms to Lewis acid sites) and PY titrates both Brønsted and Lewis acidity in the materials. The difference between the amount of PY (total acidity) and DMPY (Brønsted acidity) adsorbed should, therefore, correspond to the Lewis acidity in the materials.

Catalytic experiments

Typically, toluene (2 mL), benzyl chloride (0.2 mL) and catalyst (0.025 g) were added to a Pyrex vial and microwaved by using a pressure-controlled CEM-Discover microwave reactor for 3 min at 300 W (the maximum temperature reached was 110–120 °C) under continuous stirring. Samples were then withdrawn from the reaction mixture and analysed by GC by using an Agilent 6890N system equipped with a capillary column HP-5 (30 m × 0.32 mm × 0.25 μm) and a flame ionisation detector (FID). The identity of the products was confirmed by GC–MS. The microwave method was generally temperature controlled (by an IR probe), and the samples were irradiated with the required power output (set at maximum power, 300 W) to achieve the desired temperature.

Acknowledgements

R.L. gratefully acknowledges support from the Spanish MICINN by the concession of a RyC contract (ref. RYC-2009-04199) and fund-

ing under projects P10-FQM-6711 (Consejería de Ciencia e Innovación, Junta de Andalucía) and CTQ2011 28954-CO2-02 (MICINN). Both R.L. and J.G.M. acknowledge support from MICINN under cooperation project CTQ2011-28954. J.G.M. gratefully acknowledges funding under the WAVES project (Spanish MINECO and UE, ERA-NET CAPITA).

Keywords: alkylation · mesoporous materials · nanoparticles · supported catalysts · zeolites

- [1] J. Kärger, R. Valiullin, *Chem. Soc. Rev.* **2013**, *42*, 4172–4197.
- [2] J. Pérez-Ramírez, C. H. Christensen, K. Egeblå, C. H. Christensen, J. C. Groen, *Chem. Soc. Rev.* **2008**, *37*, 2530–2542.
- [3] a) C. H. Christensen, K. Johannsen, E. Törnqvist, I. Schmidt, H. Topsøe, C. H. Christensen, *Catal. Today* **2007**, *128*, 117–122; b) A. Silvestre-Albero, A. Grau-Atienza, E. Serrano, J. Silvestre-Albero, J. Garcia-Martinez, *Catal. Commun.* **2014**, *44*, 35–39.
- [4] M. Ogura, S. Y. Shinomiya, J. Tateno, Y. Nara, E. Kikuchi, M. Matsukata, *Chem. Lett.* **2000**, 882–883.
- [5] J. C. Groen, J. C. Jansen, J. A. Moulijn, J. Pérez-Ramírez, *J. Phys. Chem. B* **2004**, *108*, 13062–13065.
- [6] L. Zhao, J. Gao, C. Xu, B. Shen, *Fuel Process. Technol.* **2011**, *92*, 414–420.
- [7] J. C. Groen, J. A. Moulijn, J. Perez-Ramirez, *J. Mater. Chem.* **2006**, *16*, 2121–2131.
- [8] K. Sadowska, A. Wach, Z. Olejniczak, P. Kustrowski, J. Datka, *Microporous Mesoporous Mater.* **2013**, *167*, 82–88.
- [9] I. I. Ivanova, E. E. Knyazeva, *Chem. Soc. Rev.* **2013**, *42*, 3671–3688.
- [10] C. Perego, R. Millini, *Chem. Soc. Rev.* **2013**, *42*, 3956–3976.
- [11] G. Bellussi, A. Carati, C. Rizzo, R. Millini, *Catal. Sci. Technol.* **2013**, *3*, 833–857.
- [12] D. P. Serrano, J. M. Escola, P. Pizarro, *Chem. Soc. Rev.* **2013**, *42*, 4004–4035.
- [13] K. Na, M. Choi, R. Ryoo, *Microporous Mesoporous Mater.* **2013**, *166*, 3–19.
- [14] Y. Tao, H. Kanoh, L. Abrams, K. Kaneko, *Chem. Rev.* **2006**, *106*, 896–910.
- [15] J. Garcia-Martinez, M. Johnson, J. Valla, K. Li, J. Y. Ying, *Catal. Sci. Technol.* **2012**, *2*, 987–994.
- [16] J. Garcia-Martinez, K. Li, G. Krishnaiah, *Chem. Commun.* **2012**, *48*, 11841–11843.
- [17] L. Su, L. Liu, J. Zhuang, H. Wang, Y. Li, W. Shen, Y. Xu, X. Bao, *Catal. Lett.* **2003**, *91*, 155–167.
- [18] D. Verboekend, S. Mitchell, M. Milina, J. C. Groen, J. Pérez-Ramírez, *J. Phys. Chem. C* **2011**, *115*, 14193–14203.
- [19] a) L. Zhou, M. Shi, Q. Cai, L. Wu, X. Hu, X. Yang, C. Chen, J. Xu, *Microporous Mesoporous Mater.* **2013**, *169*, 54–59; b) M. Spangenberg Holm, E. Taarning, K. Egeblad, C. H. Christensen, *Catal. Today* **2011**, *168*, 3–16.
- [20] a) J. Perez-Ramirez, F. Kapteijn, J. C. Groen, A. Domenech, G. Mul, J. A. Moulijn, *J. Catal.* **2003**, *214*, 33; b) T. Tang, C. Yin, L. Wang, Y. Ji, F.-S. Xiao, *J. Catal.* **2008**, *257*, 125; c) Q. Huo, T. Dou, Z. Zhao, H. Pan, *Appl. Catal. A* **2010**, *381*, 101; d) A. L. Kustov, T. W. Hansen, M. Kustova, C. H. Christensen, *Appl. Catal. B* **2007**, *76*, 311; e) H. Jin, M. B. Ansari, S. E. Park, *Catal. Today* **2014**, DOI: 10.1016/j.cattod.2014.05.021.
- [21] *Nanocatalysis Synthesis and Applications* (Eds.: V. Polshettiwar, T. Asefa), Wiley, **2013**.
- [22] P. Kalita, N. M. Gupta, R. Kumar, *J. Catal.* **2007**, *245*, 338–345.
- [23] a) A. M. Balu, A. Pineda, K. Yoshida, J. M. Campelo, P. L. Gai, R. Luque, A. A. Romero, *Chem. Commun.* **2010**, *46*, 7825–7827; b) A. Pineda, A. M. Balu, J. M. Campelo, A. A. Romero, D. Carmona, F. Balas, J. Santamaria, R. Luque, *ChemSusChem* **2011**, *4*, 1561–1565.
- [24] a) J. C. Groen, J. C. Jansen, J. A. Moulijn, J. Pérez-Ramírez, *J. Phys. Chem. B* **2004**, *108*, 13062–13065.
- [25] F. Thibault-Starzyk, I. Stan, S. Abello, A. Bonilla, K. Thomas, C. Fernandez, J. P. Gilson, J. Perez-Ramirez, *J. Catal.* **2009**, *264*, 11–14.
- [26] a) G. Salazar-Alvarez, J. Sort, A. Uheida, M. Muhammed, S. Suriñach, M. D. Baró, J. Nogués, *J. Mater. Chem.* **2007**, *17*, 322–328; b) *Handbook of X-Ray Photoelectron Spectroscopy* (Ed.: C. D. Wagner, W. N. Riggs, L. E. Davis, G. F. Moulder, G. E. Muilenberg), PerkinElmer, Eden Prairie, **1979**; c) X. Deng, J. Lee, D. Matraga, *Surf. Sci.* **2010**, *604*, 627–632.

- [27] J. M. Campelo, D. Luna, R. Luque, J. M. Marinas, A. A. Romero, J. J. Calvino, M. P. Rodriguez-Luque, *J. Catal.* **2005**, *230*, 327–338.
- [28] Q. Zhao, W.-H. Chen, S.-J. Huang, Y.-C. Wu, H.-K. Lee, S.-B. Liu, *J. Phys. Chem. B* **2002**, *106*, 4462–4469.
- [29] B. Gil, L. Mokrzycki, B. Sulikowski, Z. Olejniczak, S. Walas, *Catal. Today* **2010**, *152*, 24–32.
- [30] D. Tzoulaki, A. Jentys, J. Perez-Ramirez, K. Egeblad, J. A. Lercher, *Catal. Today* **2012**, *198*, 3–11.
- [31] M. Milina, S. Mitchell, Z. D. Trinidad, D. Verboekend, J. Perez-Ramirez, *Catal. Sci. Technol.* **2012**, *2*, 759–766.
- [32] M. Ojeda, A. Pineda, A. A. Romero, V. Barron, R. Luque, *ChemSusChem* **2014**, DOI: 10.1002/cssc.201400055.
- [33] A. N. Tsvigunov, A. V. Apolenis, V. E. Annikov, V. M. Raikova, *Glass Ceram.* **2007**, *64*, 429–436.
- [34] P. Gupta, D. Kumar, O. Parkash, A. K. Jha, *Bull. Mater. Sci.* **2013**, *36*, 859–868.
- [35] A. Pineda, A. M. Balu, J. M. Campelo, R. Luque, A. A. Romero, J. C. Serrano-Ruiz, *Catal. Today* **2012**, *187*, 65–69.
- [36] A. M. Balu, A. Pineda, D. Obermayer, A. A. Romero, C. O. Kappe, R. Luque, *RSC Adv.* **2013**, *3*, 16292–16295.
- [37] M. M. Moghaddam, B. Pieber, T. Glasnov, *ChemSusChem* **2014**, ##DOI: 10.1002/cssc.201402455.

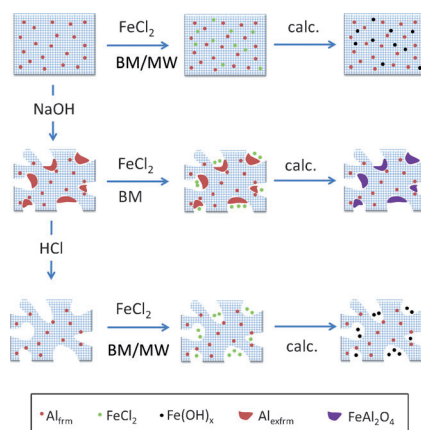
Received: July 19, 2014

Revised: August 12, 2014

Published online on ■ ■ ■, 0000

FULL PAPERS

Iron out the creases: Supported iron oxide nanoparticles are incorporated on hierarchical zeolites by microwave-assisted impregnation and mechanochemical grinding. The catalytic activities of the synthesized nanomaterials are investigated in the alkylation of toluene with benzyl chloride under microwave irradiation.



A. Grau-Atienza, R. Campos, E. Serrano, M. Ojeda, A. A. Romero, J. Garcia-Martinez,* R. Luque*



Insights into the Active Species of Nanoparticle-Functionalized Hierarchical Zeolites in Alkylation Reactions